




Bladder cancer intrinsic LRFN2 drives anticancer immunotherapy resistance by attenuating CD8⁺ T cell infiltration and functional transition

Anze Yu,¹ Jiao Hu,² Liangmin Fu,¹ Gaowei Huang,¹ Dingshan Deng,² Mingxiao Zhang,¹ Yinghan Wang,¹ Guannan Shu,¹ Lanyu Jing,³ Huihuang Li,² Xu Chen,¹ Taowei Yang,¹ Jinhuan Wei,¹ Zhenhua Chen ,¹ Xiongbing Zu ,² Junhang Luo ¹

To cite: Yu A, Hu J, Fu L, *et al.* Bladder cancer intrinsic LRFN2 drives anticancer immunotherapy resistance by attenuating CD8⁺ T cell infiltration and functional transition. *Journal for ImmunoTherapy of Cancer* 2023;11:e007230. doi:10.1136/jitc-2023-007230

► Additional supplemental material is published online only. To view, please visit the journal online (<http://dx.doi.org/10.1136/jitc-2023-007230>).

AY, JH, LF, GH and DD contributed equally.

Accepted 07 September 2023



© Author(s) (or their employer(s)) 2023. Re-use permitted under CC BY-NC. No commercial re-use. See rights and permissions. Published by BMJ.

For numbered affiliations see end of article.

Correspondence to

Professor Junhang Luo;
luojunh@mail.sysu.edu.cn

Professor Xiongbing Zu;
zuxbxy@csu.edu.cn

Dr Zhenhua Chen;
chenzh75@mail.sysu.edu.cn

ABSTRACT

Background Immune checkpoint inhibitor (ICI) therapy improves the survival of patients with advanced bladder cancer (BLCA); however, its overall effectiveness is limited, and many patients still develop immunotherapy resistance. The leucine-rich repeat and fibronectin type-III domain-containing protein (LRFN) family has previously been implicated in regulating brain dysfunction; however, the mechanisms underlying the effect of LRFN2 on the tumor microenvironment (TME) and immunotherapy remain unclear.

Methods Here we combined bulk RNA sequencing, single-cell RNA sequencing, ProcartaPlex multiple immunoassays, functional experiments, and TissueFAXS panoramic tissue quantification assays to demonstrate that LRFN2 shapes a non-inflammatory TME in BLCA.

Results First, comprehensive multiomics analysis identified LRFN2 as a novel immunosuppressive target specific to BLCA. We found that tumor-intrinsic LRFN2 inhibited the recruitment and functional transition of CD8⁺ T cells by reducing the secretion of pro-inflammatory cytokines and chemokines, and this mechanism was verified *in vitro* and *in vivo*. LRFN2 restrained antitumor immunity by inhibiting the infiltration, proliferation, and differentiation of CD8⁺ T cells *in vitro*. Furthermore, a spatial exclusivity relationship was observed between LRFN2⁺ tumor cells and CD8⁺ T cells and cell markers programmed cell death-1 (PD-1) and T cell factor 1 (TCF-1). Preclinically, LRFN2 knockdown significantly enhanced the efficacy of ICI therapy. Clinically, LRFN2 can predict immunotherapy responses in real-world and public immunotherapy cohorts. Our results reveal a new role for LRFN2 in tumor immune evasion by regulating chemokine secretion and inhibiting CD8⁺ T-cell recruitment and functional transition.

Conclusions Thus, LRFN2 represents a new target that can be combined with ICIs to provide a potential treatment option for BLCA.

BACKGROUND

Bladder cancer (BLCA) is one of the 10 most common urological malignancies worldwide.¹ Currently, neoadjuvant chemotherapy (NAC)

WHAT IS ALREADY KNOWN ON THIS TOPIC

⇒ Immune checkpoint inhibitor (ICI) therapy improves the survival of patients with advanced bladder cancer; however, its effectiveness is limited.

WHAT THIS STUDY ADDS

⇒ We firstly found that bladder cancer-intrinsic leucine-rich repeat and fibronectin type-III domain-containing protein 2 inhibited the recruitment and functional transition of CD8⁺ T cells by reducing the secretion of pro-inflammatory cytokines and chemokines.

HOW THIS STUDY MIGHT AFFECT RESEARCH, PRACTICE OR POLICY

⇒ Our results identify LRFN2 as a new target in combination with ICIs, providing a potential treatment option for bladder cancer.

combined with surgical treatment is recommended for the standard treatment option for muscle-invasive bladder cancer (MIBC) without distant metastasis; however, almost half of all patients with MIBC die owing to tumor recurrence or progression.^{2–3} Therefore, systematic comprehensive treatment is often considered an important therapy for advanced BLCA.^{4,5} Among them, the application of immune checkpoint inhibitors (ICIs) in patients with MIBC showed considerable survival benefits and fewer toxic side effects compared with chemotherapy.^{3–6,10} Therefore, ICI therapy has been recognized as a first-line adjuvant therapy for MIBC in multiple guidelines.^{3–6} However, many patients failed to respond to ICIs owing to immunotherapy resistance; therefore, new biomarkers must be identified to overcome immunotherapy resistance, predict ICI responses, and develop new therapeutic targets.

The tumor microenvironment (TME) determines the occurrence of tumor immune responses.^{11–12} According to the infiltration of immune cells, the TME can be divided into three categories: (1) immune desert, (2) immune-excluded, and (3) immune inflammatory phenotypes.^{13,14} Among them, the immune inflammatory phenotype tends to have a better prognosis and a higher response to ICIs.^{15–16} The principle is that ICIs act on tumor-infiltrating TCF-1⁺PD-1⁺CD8⁺ T cells (also known as precursor exhausted T cells) to promote their proliferation and transition into TCF-1⁺PD-1⁺CD8⁺ T cells (also known as terminally exhausted T cells) with a stronger cytotoxic effect.¹⁵ TCF-1⁺PD-1⁺ precursor-exhausted CD8⁺ tumor infiltrating lymphocytes (TILs) can self-renew and transition into TCF-1⁺PD-1⁺ terminally exhausted TILs to achieve antitumor immunity. Regarding the immune desert and immune-excluded phenotypes, they lack sufficient immune cell infiltration to effectively respond to ICIs and thus often result in immunotherapy resistance.^{14–17–19} Inspired by this, we seek to identify a new treatment target that can increase immune infiltration and potentially be used in combination with ICIs to enhance immunotherapy efficacy.

The leucine-rich repeat and fibronectin type-III domain-containing protein (LRFN) family has been reported to be involved in regulating neuronal and synaptic development of the cell adhesion molecule family and has also been associated with brain dysfunction^{20–24}; however, its role in the TME and immunotherapy remains unclear, especially in BLCA. Therefore, in this study, we performed comprehensive multiomics analyses of indicators related to the TME in multiple public BLCA cohorts and our center's BLCA cohort.²⁵ We found for the first time that LRFN2 inhibits the immune response in TME. Thus, we explored the underlying molecular mechanism and found that LRFN2 blocked the infiltration of cytotoxic T cells into TME by inhibiting cytokine-related and chemokine signaling pathways using RNA sequencing. Multiple *in vitro* analyses showed a stable negative correlation between chemokine/cytokine secretion and LRFN2 expression. Through tissue microarray (TMA) panoramic analysis, we found that CD8, PD-1, and TCF-1 were mutually exclusive with LRFN2⁺ tumor cells in spatial distribution. *In vivo*, LRFN2 deficiency increases CD8⁺ T-cell infiltration and promotes differentiation toward TCF-1⁺PD-1⁺ terminally exhausted T cells, which shows a higher antitumor ability and synergistic effect with ICIs therapy. More importantly, our real-world BLCA immunotherapy cohort and public immunotherapy cohort validated the role of LRFN2 in predicting immunotherapy efficacy.

MATERIALS AND METHODS

Study design

Xiangya cohort

As we previously reported,^{2–25–26} RNA sequencing (RNA-seq) of qualified samples from 57 eligible patients with BLCA and 13 paired untreated adjacent normal samples

were collected from Xiangya Hospital (GSE188715). Three samples of muscle-invasive BLCA were collected for single-cell RNA (scRNA) sequencing and named the Xiangya scRNA cohort. In addition, we constructed two TMAs containing 50 BLCA samples without prior treatment and 51 BLCA samples with neoadjuvant immune checkpoint blockade therapy. We named these two cohorts the Xiangya BLCA and Xiangya immunotherapy cohorts.

Public database

The Cancer Genome Atlas (TCGA) database, RNA expression matrices, and survival outcomes for 33 cancers were downloaded from the UCSC Xena data portal (<https://xenabrowser.net/>). For TCGA-BLCA, we normalized RNA-seq data by log₂ transformation, and the GISTIC algorithm was used to process CNV data. We used the “GEOquery” R package to download GSE32894, GSE13507, GSE70691, GSE48075, GSE48276, GSE120736, GSE104922, GSE52219, GSE52329, and GSE69795. IMvigor210 cohort were obtained from Mariathasan *et al.*⁸ Single-cell transcriptomic data for the BLCA scRNA cohort, GSE135337 (eight samples), were downloaded from the Gene expression omnibus (GEO) database. The data processing was similar to that of the Xiangya scRNA cohort.

Calculation of TME cell infiltration in BLCA

As we previously described,^{2–25–27} we comprehensively evaluated the immunological properties of the TME in BLCA. We evaluated the activities of the seven-step cancer immunity cycles to reveal antitumor immunity effectiveness in the TME. The infiltration levels of immune cells were calculated based on seven algorithms (ssGSEA, TIMER, CIBERSORT, CIBERSORT-abs, MCP-counter, TISIDB, and xCell). Based on a study by Charoentong *et al.*,²⁸ we collected effector genes, chemokine ligands and receptors, MHC (major histocompatibility complex) molecules, and immune stimulators of immune cells to evaluate immune properties. According to Auslander *et al.*²⁹ and Ayers *et al.*,³⁰ T-cell inflammation scores (TIS) and immune checkpoint blockade markers (ICBs) were used to assess the state of immunotherapy sensitivity.

Enrichment pathways analyses

As described previously,²⁵ differentially expressed genes (DEGs) in bulk RNA-seq data were filtered by Limma R package, with a screening threshold for |log (fold change) >1 and adjusted p value <0.05. The Seurat R package and FindMarker algorithms were used to identify genes specifically expressed in the scRNA sequencing data. Gene Ontology (GO) and Kyoto Encyclopedia of Genes and Genomes (KEGG) were used to analyze the identified DEGs using the ClusterProfiler R package.

Identifying the BLCA molecular subtype of individuals

At present, there are seven main molecular subtype models of BLCA, including North Carolina (UNC), MDA, Cartes d'Identite des tumor-curie (CIT), Lund, TCGA

and Baylor, and Consensus subtypes. These molecular subtypes have been widely used to evaluate the characteristics and efficacy of various treatments. Consensus MIBC and BLCA subtyping algorithms were used to classify the above molecular subtypes in patients with BLCA into basal and luminal subtypes. The accuracy of LRFN2 in predicting molecular subtypes was tested by an Receiver Operating Characteristic (ROC) curve analysis.

Cell lines and cell culture

T24 human BLCA cells were obtained from the American Type Culture Collection (ATCC, Manassas, Virginia, USA). Mouse BLCA cells (MB49) were kindly gifted by Dr Jian Huang from the Sun Yat-sen Memorial Hospital. The cell culture was performed in Dulbecco's modified eagle medium (Gibco) containing 10% fetal bovine serum (Gibco), 1% penicillin and streptomycin (Invitrogen). The condition of the incubator was set as 37°C with 5% CO₂. All cell lines were identified by a short tandem repeat DNA assay and tested negative for *Mycoplasma* contamination.

Stable cell line construction and RNA-seq

The LRFN2-shRNA (shRNA) plasmid was constructed using GK (GK Biotechnology). The target sequences were as follows: sh-LRFN2 #Human 1: 5'-GGACCGCTGTCTATGACAA-3' sh-LRFN2 #Human 2: 5'-GCATGCTCTTGCCCTTTGA-3' sh-LRFN2 #Mouse 1: 5'-GGACTGCTGTATATGACAATG-3' sh-LRFN2 #Mouse 2: 5'-GCACCCTGGACATTCTAATTA-3'

The lentiviral packaged plasmid and negative control plasmid were purchased from GeneCopoeia (Rockville, Maryland, USA). Human 293T cells were transfected with human and mouse LRFN2-shRNA plasmids using Lipofectamine 2000 (Invitrogen). At 48 hours after transfection, the supernatant containing human and mouse LRFN2 shRNA lentivirus was collected and transfected into T24 and MB49 cells, respectively. Puromycin (3 µg/mL; Amersco, USA) was used to select stably transfected cell lines. Western blotting and quantitative reverse transcription PCR (qRT-PCR) were used to verify the transfection effect and the detailed methods were mentioned as we previously described.²⁵ Three duplicate samples from the T24 cell line were analyzed using the Beijing Genomics Institute RNA-seq platform (Shenzhen, China). The selection criteria and enrichment pathway analysis of the DEGs were the same as those used in previous studies.

ProcartaPlex immunoassay plate

Cell culture supernatants from stably transfected cancer cells were used to detect the protein expression levels of chemokines and cytokines. In brief, cell culture supernatants were collected and cell debris were removed by centrifugation, and the human ProcartaPlex immunoassay plate (Cat: EPX340-12163-901, Thermo Fisher Scientific) and mouse immunoassay panel ProcartaPlex (Cat: EPX360-26092-901, Thermo Fisher Scientific) were used. For the stimulation experiment, the cell culture system was added with human interferon (IFN)-γ (PeproTech)

or human tumor necrosis factor (TNF)-α (PeproTech) for 12 hours before supernatants collection. Each sample was quantitatively analyzed using the Luminex Detection Platform (Thermo Fisher Scientific, USA).

Western blot

In brief, Radio Immunoprecipitation Assay Lysis buffer supplemented with 1% protease inhibitor was used to lysis total proteins from cells or tissues. BCA Protein Assay Kit (NCM Biotech, China) was used to analyze protein concentrations. Primary antibodies and horseradish peroxidase (HRP)-conjugated secondary antibodies were used to incubate with the transferred PVDF (Polyvinylidene fluoride) membranes. The signals were captured using a Western Blot Substrate Kit (Tanon, Shanghai, China). The primary antibodies included anti-LRFN2 (Cat: TA306739, OriGene, USA), anti-GAPDH (Cat: ab8245, Abcam, USA), anti-Ikkα+β antibody (Cat: ET1611-23, HUABIO, China), anti-p65 (Cat: ER0815, HUABIO, China), anti-p-p65 (Cat: ET1604-27, HUABIO, China), anti-IKB-α (Cat: ET1603-6, HUABIO, China), anti-p-IKB-α (Cat: ET1609-78, HUABIO, China) and anti-Tubulin (Cat: 10068-1-AP, ProteinTech, USA). The secondary antibodies included HRP goat anti-rabbit IgG (Cat: 7074, Cell Signaling Technology, USA) and HRP goat anti-mouse IgG (Cat: 7076, Cell Signaling Technology, USA).

T-cell separation, activation, and culture

Briefly, blood samples of healthy donors were used to isolate peripheral blood mononuclear cells (PBMCs). Fresh blood samples were diluted with phosphate-buffered saline (PBS) and separated using Ficoll-Paque (Cat: 17-1400-03, GE HealthCare, USA) via gradient centrifugation. For human T-cell activation, ImmunoCult Human CD3/CD28/CD2 T-cell activator (Cat: 10970; STEMCELL Technologies, USA) was used to activate PBMCs. Human T-cell medium supplemented with Recombinant Human IL-2 Protein (Cat: 202-1L-050, R&D, USA) was used for human T-cell culture.

Splenocytes were obtained from the spleens of C57B/L6 mice, and RBC (red blood cells) were lysed using ACK lysis buffer (Cat: A1049201, Gibco, USA). The splenocytes were activated with mouse-CD3 (Cat: 05112-25-500, BioGems, USA)-incubated plates and cultured in mouse T-cell medium.

Co-culture assay and LDH assay

T24-shNC, T24-shLRFN2-1 and T24-shLRFN2-2 were co-cultured with activated human T cells from a healthy donor in a 12-well plate for 12–72 hours. MB49-shNC, MB49-shLRFN2-1 and MB49-shLRFN2-2 were co-cultured with activated mouse T cells from C57B/L6 mice. The supernatants were collected for the LDH assay (Cat: 88954, Thermo Fisher, USA) according to the manufacturer's protocol. T cells were collected and stained with antibodies for flow cytometry analysis. The remaining cancer cells were counted daily to determine the number of remaining cells.

CD8⁺ T-cell migration assay

In brief, we used the Human CD8⁺ T Cell Isolation Kit (Cat: 480012, BioLegend, USA) to isolate human CD8⁺ T cells according to the manufacturer's protocol. EasySep Mouse CD8⁺ T Cell Isolation Kit (Cat: 19853, STEMCELL, USA) was used to isolate mouse CD8⁺ T cells according to the manufacturer's protocol. A 24-well transwell system with a 6.5 mm diameter and 3 μm pore size polycarbonate membrane (Corning, USA) was used to perform the CD8⁺ T-cell migration assay. The lower chambers were added with supernatant (500 μL) from the T24-shNC and T24-shLRFN2 transferred cell lines, whereas the upper chambers were added with 1×10⁵ isolated CD8⁺ T cells. The number of CD8⁺ T cells that migrated to the lower layer was measured using a cell counting plate after incubation for 6 hours at 37°C.

In vivo experiments

Female C57BL/6 mice aged 6–8 weeks were purchased from Vital River Company. In the subcutaneous tumorigenesis model, 5×10⁵ MB49-shNC/MB49-shLRFN2 cells were injected into the right flank of each mouse. For the immunotherapy model, 100 μg anti-mouse PD-1 (Cat: BE0146, Bio X Cell, USA) or IgG2a isotype (Cat: BE0089, Bio X Cell, USA) was injected intraperitoneally when the tumors could be touched. The drugs were injected two times every 3 days. Vernier caliper was used to measure tumor volume every 2 days.

For the in situ intravesical tumorigenesis model, 5×10⁵ MB49-shNC-luci/MB49-shLRFN2-luci cells were injected into the bladder through the catheter after passing urine. In vivo mouse imaging was performed on day 18 via intraperitoneal injection of luciferase to observe the tumor volume using the IVIS system (PerkinElmer, USA). Mice were euthanized at the end of the experiment, or the endpoint of animal ethics was reached.

TissueFAXS panoramic analyses

To evaluate the relationship between LRFN2⁺ malignant cells, CD8⁺ T cells, and effector T-cell molecules, we used the TissueFAXS panoramic (TissueGnostics, Austria) to detect the expression of target cells and molecules stained by multiple immunofluorescences in biopsies from tumor tissues in the Xiangya BLCA TMA Cohort and Xiangya immunotherapy cohort. In Brief, specific primary and secondary antibodies were used to stain LRFN2⁺ cells, BLCA cells, PD-1⁺ cells, and TCF-1⁺ cells. Tumor cells were stained with the CK19 antibody. Cell nuclei were stained with DAPI (Invitrogen, USA), as described by Makarevic *et al.*³¹ For spatial analysis, CD8⁺ T cells, PD-1⁺ cells, and TCF-1⁺ cells around LRFN2⁺CK19⁺ cells are quantified according to the distance gradients (0–25 μm, 25–50 μm, 50–100 μm, and 100–150 μm).

Tumor infiltrating T-cell extraction

The tumors were excised, and sliced into small pieces in sterile containers after euthanizing the mice. The tumors were digested in RPMI1640 solution containing

collagenase I, hyaluronidase, and DNase for 45 min, followed by washing with sterile PBS. Lymphoprep (STEMCELL, USA) was used to extract the TILs by gradient centrifugation at 2000×g for 15 min. Extracted TILs were stored for subsequent experiments.

Flow cytometry analysis

BV421-Zombie Aqua Fixable Viability Kit (Cat: 423102, BioLegend, USA) was used to stain mouse splenocytes and TILs for 15 min at room temperature to eliminate the impact of dead cells. For surface marker staining, mouse splenocytes and TILs were stained with FITC-anti-mouse CD45 (Cat: 30-F11, BioLegend), PerCP-Cy5.5-anti-mouse CD8 (Cat: 53–6.7, BioLegend), Pacific Blue-anti-mouse CD4 (Cat: GK1.5, BioLegend), PE-anti-mouse PD-1 (Cat: 29F.1A12, BioLegend), PE-anti-mouse Tim-3 (Cat: RMT3-23, BioLegend), APC-anti-mouse TIGIT (Cat: 1G9, BioLegend), PE-anti-mouse CD44 (Cat: IM7, BioLegend), or APC-anti-mouse CD62L (Cat: MEL-14, BioLegend) for 15 min at room temperature. For transcription factor staining, mouse splenocytes and TILs were fixed and permeabilized using Fix/Perm buffer at 25°C for 1 hour, then stained with APC-anti-mouse/human TCF-1 (Cat: C63D9, Cell Signaling Technology), or PE-anti-mouse Ki-67 (Cat: 16A8, BioLegend) for 30 min at room temperature. For cytokine staining, TILs were incubated in RPMI-1640 medium supplemented with Phorbol 12-myristate 13-acetate (Cat: M4647, AbMole), ionomycin (Cat: M3621, AbMole), and GolgiStop (Cat: M6991, AbMole) for 4 hours. TILs were then stained with Zombie Aqua Dye according to the above protocol. Fix/Perm buffer (Cat: FC007, R&D) was used for the fixation and permeabilization. TILs at 4°C overnight and TILs were stained with PE-anti-mouse IFN-γ (Cat: XMG1.2, BioLegend) and APC-anti-mouse TNF-α (Cat: MP6-XT22, BioLegend) for 1 hour at 4°C. BD LSRFortessa was used to detect stained cells, and FlowJo software (V.10.8.1) was used to analyze the data.

Statistical analyses

For continuous variables, we used an independent sample t-test or Mann-Whitney U test to compare parameters between the two groups. For dichotomous variables, we used the χ^2 test or Fisher's exact test to compare the differences. For the correlation between different variables, Pearson or Spearman correlation coefficient tests were used. We used the Kaplan-Meier survival curve to show prognostic analyses of dichotomous variables, and the log-rank test to assess the significance. GraphPad Prism V.8 (GraphPad Software) and R software (V.4.0) were used for data analyses. Values of p<0.05 were recognized as statistical significance.

RESULTS

Comprehensive analysis of LRFN2's role in bladder cancer TME

LRFN2 expression is higher in most cancers compared with normal tissues (online supplemental figure S1A),

and such expression is also observed in BLCA, and this phenomenon was also verified in our Xiangya cohort (online supplemental figure S1B). Our results revealed that LRFN2 had the most evident immunosuppressive effect in BLCA (online supplemental figure S2A). The analysis exploring the association between LRFN2 and various immune cells revealed a markedly negative correlation in BLCA (online supplemental figure S2B). In addition, LRFN2 expression was negatively correlated with immune checkpoints PD-1, programmed cell death ligand 1 (PD-L1), cytotoxic T-lymphocyte antigen 4 (CTLA-4), and lymphocyte-activation gene 3 (LAG-3) in BLCA (online supplemental figure S2C-F). We highlight the immunosuppressive effect of LRFN2 on BLCA, suggesting it should be a focus for further research.

In the TCGA-BLCA cohort, we found that LRFN2 was negatively correlated with cancer immune cycles, which involved a series of steps, including tumor antigen release, immune system recognition, immune cell recruitment, and tumor killing (figure 1A). Chemokines, receptors, MHC-related molecules, immunostimulators, and immune checkpoints were lower expressed in the high LRFN2 expression group, whereas they were overexpressed in the low LRFN2 expression group (online supplemental figure S3A-C). In addition, we found that LRFN2 expression was negatively correlated with the levels of antitumor immune cells, such as CD8⁺ T cells, CD4⁺ T cells, natural killer (NK) cells, and M1 macrophages, using six different algorithms (figure 1B). We also verified these results in the Xiangya BLCA cohort (figure 1C). Similarly, at the transcriptome level fewer immune cell effector genes were expressed in the high LRFN2 expression group, as shown in figure 1D. Moreover, T-cell inflammation scores and LRFN2 expression were considerably negatively correlated in the TCGA-BLCA cohort (figure 1E). Finally, we found that LRFN2 expression was negatively correlated with most ICI and TIS genes in the Xiangya BLCA cohort (figure 1F). This suggests that patients with higher LRFN2 expression may have non-inflamed tumors and may be less sensitive to immunotherapy.

Specifically, subtypes of BLCA include basal and luminal, which accurately reflect patient prognosis and treatment response.^{32–34} In the TCGA-BLCA cohort, LRFN2 could be used to distinguish basal types from luminal subtypes. Tumors with high LRFN2 expression belonged to the luminal classification and showed higher enrichment scores in luminal differentiation and urothelial differentiation. In contrast, tumors with low LRFN2 expression belonged to the basal classification, where enrichment scores of basal differentiation, immune differentiation, and IFN_γ response were significantly higher (online supplemental figure S5A). ROC curve results indicated that LRFN2 predicted molecular subtypes with an accuracy of more than 0.9 among the other six independent classification systems, except the Baylor classification system (online supplemental figure S5B), indicating that LRFN2 had strong predictive value

for molecular subtypes. The basal subtype (low LRFN2 group) is generally considered to have greater cytotoxic lymphocyte infiltration and show more immunotherapy sensitivity. Here, we found that multiple immune-inhibited-oncogenic pathways were significantly activated in tumors with high LRFN2 expression (online supplemental figure S5C), and previous studies have identified that activation of these pathways leads to TME formation without inflammation. The CNV analysis indicated that high LRFN2 expression corresponded to the luminal subtype, which is linked to resistance to treatments, such as NAC and ICIs, thereby increasing the risk of BLCA progression during ICI therapy (online supplemental figure S5D). Additionally, high LRFN2 expression was associated with higher ARID1A and ATM mutations, suggesting that these patients may also have resistance to NAC (online supplemental figure S5E). Further validation of these results was conducted in the DrugBank database (online supplemental figure S5F), and the findings suggest that patients with low LRFN2 expression were suitable for chemotherapy. To verify the general applicability of these findings, the Xiangya BLCA cohort was used to validate these results (not shown here) and further demonstrated in 10 public BLCA cohorts (GSE32894, GSE13507, GSE70691, GSE48075, GSE48276, imvigor210, GSE120736, GSE104922, GSE52219, GSE52329, and GSE69795, online supplemental figures S6–S16), and similar conclusions were reached. According to these results, LRFN2 expression negatively affected cytotoxic lymphocyte infiltration of the BLCA molecular subtypes and immunotherapy response. Collectively, high LRFN2 expression in BLCA corresponded to a non-inflammatory TME.

Single cell RNA sequencing and bulk RNA sequencing revealed the immunosuppressive role and potential mechanisms of LRFN2 in BLCA

Three tumor samples from patients with MIBC from Xiangya Hospital (one did not receive immunotherapy, one was resistant to immunotherapy, and one responded to immunotherapy) were collected for scRNA sequencing.²⁵ The total cells were divided into six categories: endothelial cells, myeloid cells, fibroblasts, epithelial cells, T/NK cells, and B cells (figure 2A). LRFN2 was expressed almost exclusively in malignant epithelial cells, but not in immune or stromal cells (figure 2B). By comparing the levels of LRFN2 expression in BLCA cells, high LRFN2 and low LRFN2 groups were identified. Through GO enrichment pathway analysis, a negative correlation was found between the high LRFN2 group and many immunoregulatory pathways, including the type 2 immune response, regulation of leukocyte proliferation, positive regulation of leukocyte proliferation, and regulation of leukocyte cell–cell adhesion (figure 2C). Consistently, through GO and KEGG enrichment analysis of the Xiangya bulk RNA-seq results, we found high LRFN2 expression was negatively correlated with chemokine activity, response to chemokine, chemokine production,

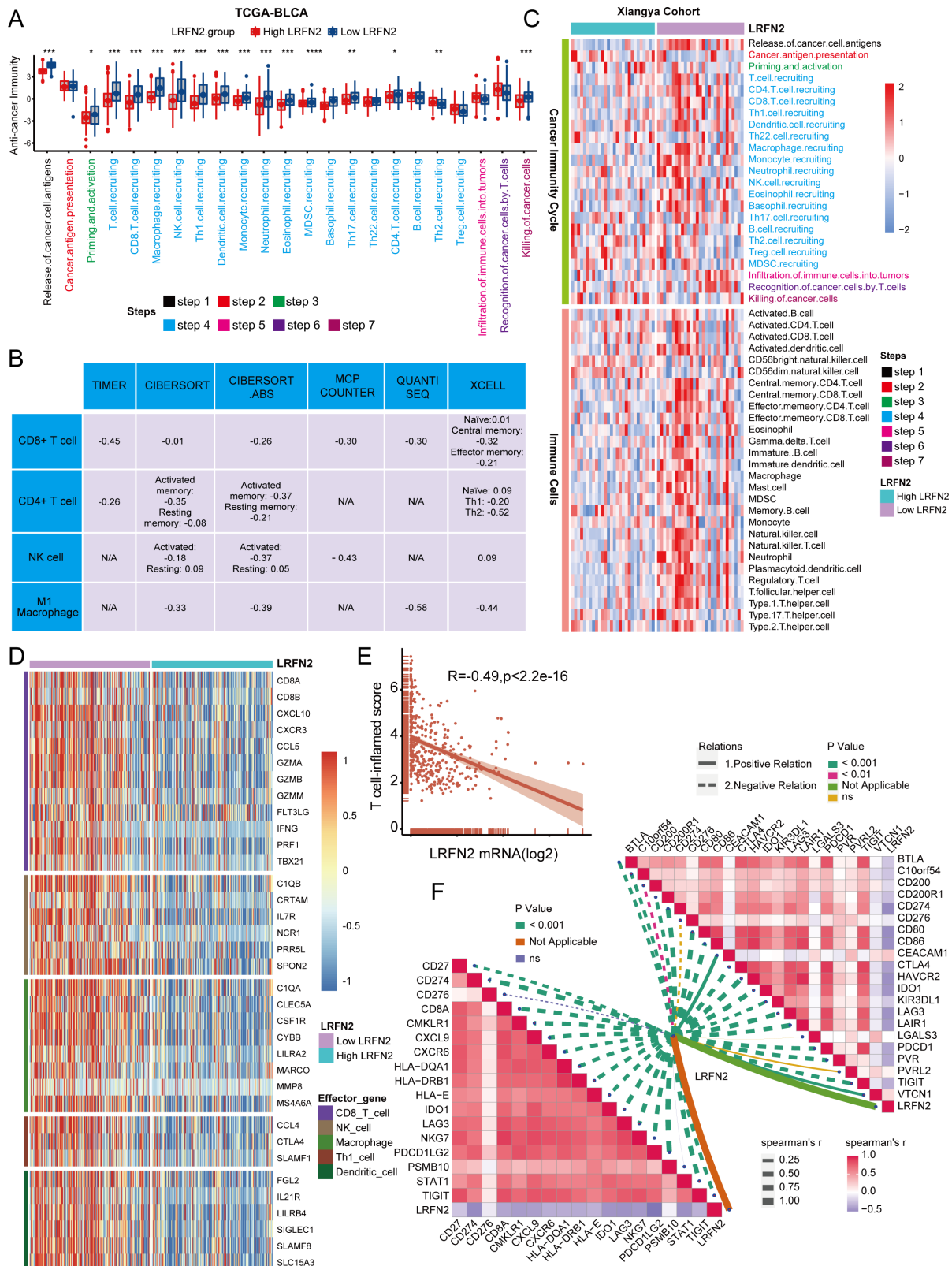


Figure 1 LRFN2 correlated with a non-inflammatory tumor microenvironment in BLCA. (A) LRFN2 expression and cancer immunity cycles in BLCA. The colors represent seven different steps. (B) LRFN2 expression and CD4⁺ T cell, CD8⁺ T cell, M1 macrophage, and NK cell infiltration levels in six independent algorithms. (C) LRFN2 expression, infiltrated immune cells and cancer immunity cycles in the Xiangya cohort. (D) Effector genes expression of CD8⁺ T cells, dendritic cells, NK cells, macrophages, and Th1 cells in high-LRFN2 and low-LRFN2 groups in TCGA-BLCA. (E) LRFN2 expression and T cell-inflamed scores in TCGA-BLCA. (F) LRFN2 expression and T cell-inflamed related genes (bottom left) and immune checkpoint genes (upper right) in the Xiangya cohort. * $p < 0.05$, ** $p < 0.01$, *** $p < 0.001$. BLCA, bladder cancer; LRFN2, leucine-rich repeat and fibronectin type-III domain-containing protein; mRNA, messenger RNA; NK, natural killer; TCGA, The Cancer Genome Atlas.

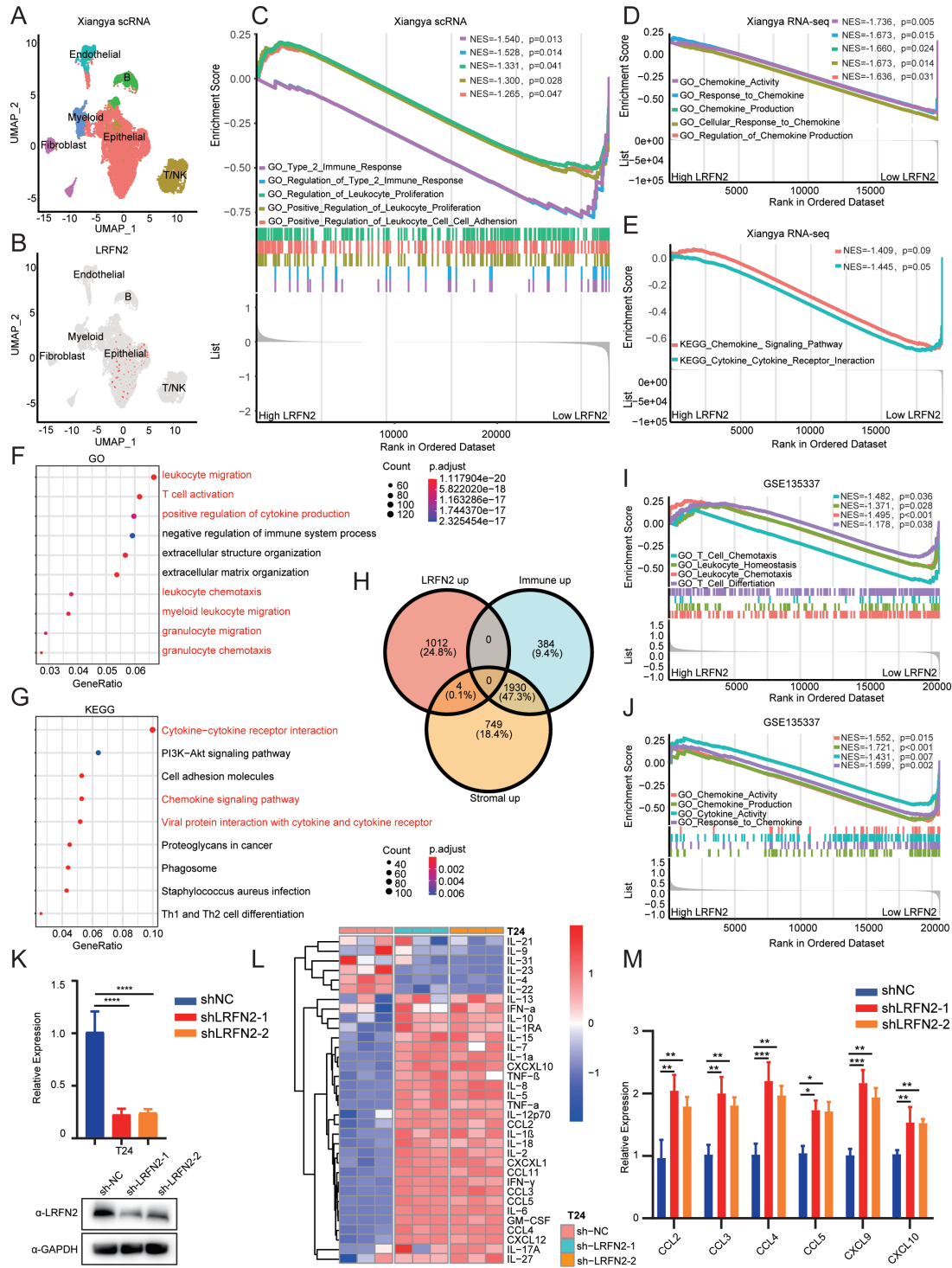


Figure 2 LRFN2 is specifically expressed in BLCA cells and inhibits cytokine and chemokine secretion. (A–B) UMAP plot of all the single cells and LRFN2 expression pattern in the Xiangya scRNA-seq. (C–D) GO enrichment between different LRFN2 expression groups in BLCA cells in the Xiangya scRNA-seq. (E) KEGG enrichment between different LRFN2 expression groups in BLCA cells in the Xiangya scRNA-seq. (F–G) KO and KEGG enrichment between different LRFN2 expression groups in TCGA-BLCA. (H) Venn diagram showed different expressed genes among high LRFN2 expression group, high immune-related genes group and high stromal score group. (I–J) GO enrichment between different LRFN2 expression groups in BLCA cells in GSE135337. (K) qRT-PCR and western blot of LRFN2 knock down in human bladder cancer cell line T24. (L) Heatmap of the chemokines/cytokines secretion in supernatants of T24-shNC and T24-shLRFN2 cells detected by ProcartaPlex multiple immunoassays. (M) qRT-PCR detected CCL2, CCL3, CCL4, CCL5, CXCL9, and CXCL10 RNA express levels in T24-shNC and T24-shLRFN2 cells. * $p < 0.05$, ** $p < 0.01$, *** $p < 0.001$, **** $p < 0.0001$. UMAP, Uniform Manifold Approximation and Projection; BLCA, bladder cancer; GO, Gene Ontology; KEGG, Kyoto Encyclopedia of Genes and Genomes; LRFN2, leucine-rich repeat and fibronectin type-III domain-containing protein; qRT-PCR, quantitative reverse transcription PCR; scRNA-seq, single cell RNA sequencing; TCGA, The Cancer Genome Atlas.

cellular response to chemokine, regulation of chemokine production, chemokine signaling pathway, and cytokine–cytokine receptor interaction (figure 2D,E).

To further improve the reliability of the sequencing results, we verified the above results in another external scRNA sequencing database for BLCA (GSE135337) and found that LRFN2 was still expressed almost exclusively in malignant urothelial cells. In the GO enrichment analysis of GSE135337, we also found high LRFN2 expression was negatively correlated with T-cell chemotaxis, leukocyte homeostasis, leukocyte chemotaxis, T-cell differentiation, chemokine production, chemokine activity, cytokine activity, and response to chemokines (figure 2I,J). A list of DEGs has been compiled and crossed among the up/down LRFN2, up/down immune score, and up/down stromal score groups in the TCGA-BLCA cohort (online supplemental figure S4B). The results showed that there were no common genes among the upregulated LRFN2, immune score, stromal score, and downregulated groups (figure 2H, online supplemental figure S4A). Based on the DEGs, we further verified the immunosuppressive effect of LRFN2 in BLCA using GO and KEGG enrichment analyses, suggesting a similar negative regulation of immune response in TCGA-BLCA (figure 2F,G).

In summary, the above results suggest that LRFN2 may contribute to the formation of a non-inflammatory TME by influencing cytokine/chemokine pathways.

LRFN2 inhibits CD8⁺ T-cell recruitment and cytotoxicity by reducing the secretion of chemokines in human BLCA cell lines

As predicted by the multiplexomics analysis, enrichment analysis from different LRFN2 expression cell lines also indicated that the cytokine/chemokine pathway was the downstream pathway of LRFN2 (online supplemental figure S17F). Therefore, cytokine/chemokine detection was conducted on the supernatant of constructed T24-shNC, T24-shLRFN2-1 and T24-shLRFN2-2 (figure 2K) using the ProcartaPlex multiplex immunoassay to identify downstream cytokines/chemokines significantly regulated by LRFN2 (figure 2L). The results showed that when LRFN2 was knocked down by two different shRNAs, significant increase in the levels of CCL2, CCL3, CCL4, CCL5, and CXCL10 were observed in T24 cells. These chemokines are considered essential in promoting immune cells recruitment and infiltration.^{35–36} The messenger RNA (mRNA) expression levels of these chemokines were detected in T24-shNC, T24-shLRFN2-1 and T24-shLRFN2-2 cell lines using qRT-PCR, and we found that *CCL2*, *CCL3*, *CCL4*, *CCL5*, *CXCL9*, and *CXCL10* mRNA expression levels significantly increased after knockdown of LRFN2 (figure 2M). Furthermore, we performed stimulation experiments using T24-shNC, T24-shLRFN2-1, T24-shLRFN2-2 cell lines stimulated with IFN- γ and TNF- α . The proteins expression level was tested by multiplex ELISA (online supplemental figure S17A,B) and mRNAs expression level of several chemokines was tested by qRT-PCR (online supplemental figure S17C,D). Notably, stimulation with typical TME factors like IFN- γ and

TNF- α significantly increased the expression of most pro-inflammatory cytokines/chemokines in LRFN2 knock down BLCA cell lines. To verify how LRFN2 reduces cytokine/chemokine expression, we assessed key signaling cascades controlling cytokine responses in Nf- κ B signaling pathway in dependence of the LRFN2 expression status. As shown in online supplemental figure 17E, after knock down of LRFN2 in T24 cells, the expression level of IKK α + β , p65, IKK α and p-IKKB α increased, and the expression level of p-p65 did not change apparently. Based on these results, it appears that LRFN2 knockdown inhibits CD8⁺ T cell-related chemokines expression at the transcriptome and proteome levels. Subsequently, through T-cell co-culture and lactate dehydrogenase (LDH) experiments, we found that T24-shLRFN2 improved the cytotoxicity of immune cells and killed tumor cells more easily compared with T24-shNC (online supplemental figure S18A-C). The in vitro T-cell migration assay showed that LRFN2 knockdown significantly increased CD8⁺ T-cell migration when compared with the negative control (online supplemental figure S18D,E).

LRFN2⁺ tumor cells negatively correlated with CD8⁺ T-cell infiltration and differentiation in human BLCA

In the above results, we demonstrated the immunosuppressive effect and potential mechanism of LRFN2 in BLCA using external databases, Xiangya bulk-RNA sequence, Xiangya scRNA sequence, and in vitro human BLCA cells. However, at the human tissue level, the correlation between LRFN2⁺ tumor cells and T cells, and the molecules involved in T-cell differentiation remains unclear. Previous studies revealed that most CD8⁺ T-cell infiltrating tumors remained in an exhaustion-like stage, and TCF-1 and PD-1 are considered key molecules in regulating CD8⁺ T-cell differentiation^{15–37–40}. TCF-1⁺PD-1⁺ precursor exhausted CD8⁺ TILs can self-renew and transit into TCF-1⁺PD-1⁺ terminally exhausted TILs to achieve antitumor immunity. Therefore, we prepared a TMA containing 50 BLCA samples, namely, the Xiangya BLCA TMA, and performed multicolor staining on LRFN2⁺ tumor cells (LRFN2⁺CK19⁺), CD8⁺ T cells, PD-1⁺ cells, and TCF-1⁺ cells. The TissueFAXS panoramic quantitative platform was used for semi-automatic analysis to reveal the spatial exclusion of LRFN2⁺ BLCA, CD8⁺ T, PD-1⁺, and CD8⁺TCF-1⁺ cells. Tumors with low LRFN2 expression exhibited inflammatory phenotypes, with a large number of CD8⁺ T cells infiltrating the tumor area, including TCF-1⁺PD-1⁺CD8⁺ precursor-exhausted T cells and TCF-1⁺PD-1⁺CD8⁺ terminally exhausted T cells (figure 3A and online supplemental figure S19A). In contrast, high expression of LRFN2 in tumor molecules (CK⁺) showed non-inflammatory phenotypes, and extensive expression of LRFN2 in tumor cells inhibited CD8⁺ T-cell infiltration and differentiation in tumor area (figure 3B and online supplemental figure S19B). Compared with the co-expression ratio of LRFN2⁺CD8⁺ T cells (0.45%) and LRFN2⁺PD-1⁺ T cells (0.63%), LRFN2 was mainly expressed in BLCA cells (44.79%), which revealed similar results as scRNA sequencing (figure 3C).

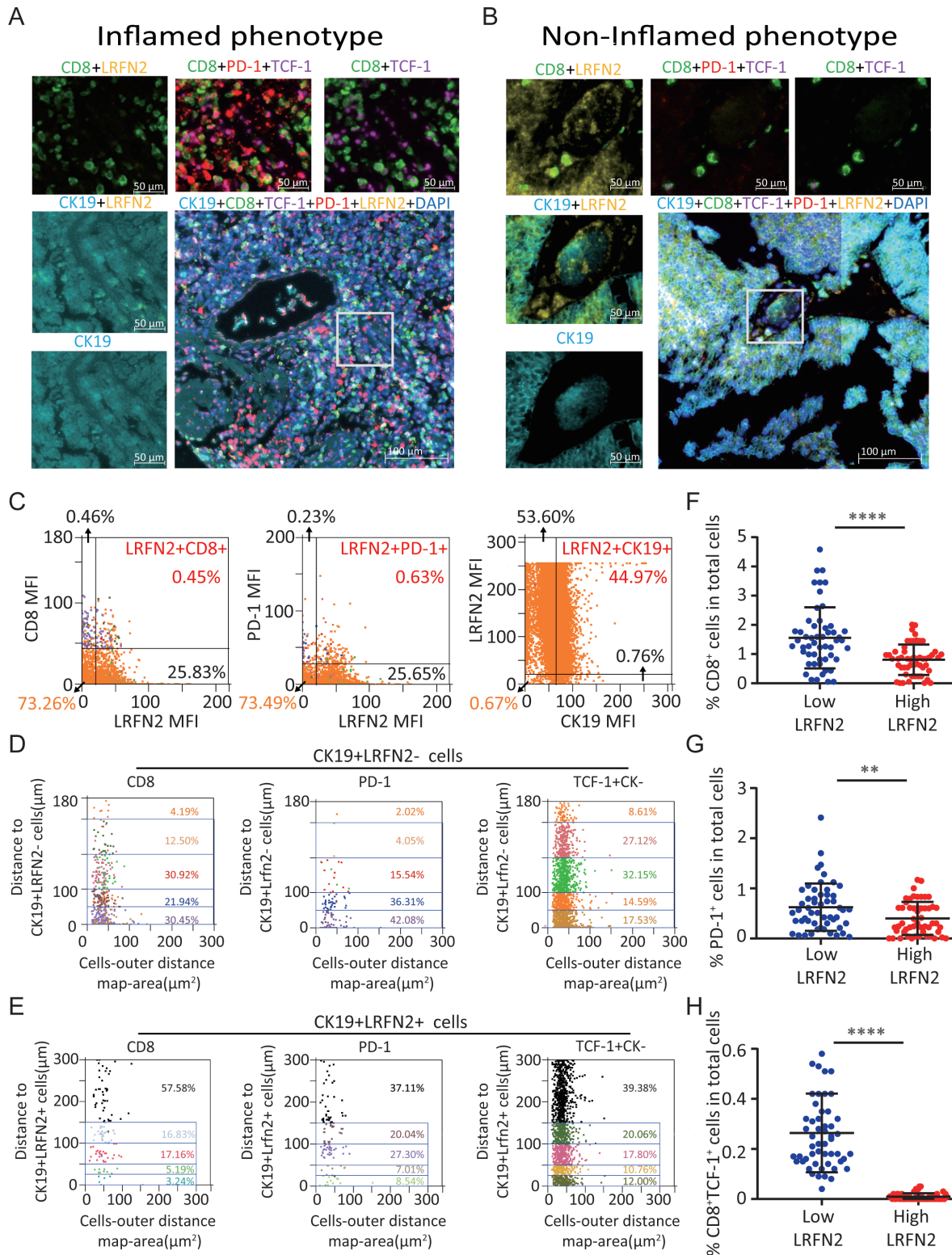


Figure 3 LRFN2⁺ tumor cells were negatively correlated with CD8⁺ T-cell infiltration and differentiation in human BLCA. (A–B) Representative multicolor staining of inflamed (A) and non-inflamed (B) phenotypes of patients with BLCA in the Xiangya BLCA tissue microarray (TMA): LRFN2 (yellow), CK19 (azure), CD8 (green), TCF-1 (purple), PD-1 (red), and DAPI (blue). (C) Representative flow cytometry-like plots of CD8⁺PD-1⁺ (left), LRFN2⁺PD-1⁺ (middle) and LRFN2⁺CK-19⁺ cells (right) in TMA, respectively. (D–E) Gradient analysis for multidimensional distances (0–25 μ m, 25–50 μ m, 50–100 μ m, 100–150 μ m) showed the spatial distribution of LRFN2⁺ tumor cells (D) and LRFN2⁻ tumor cells (E) between CD8⁺ cells, PD-1⁺ cells and CD8⁺TCF-1⁺ cells. (F–H) Percentage of CD8⁺ cells (F), PD-1⁺ cells (G), and CD8⁺TCF-1⁺ cells (H) in total cells of high-LRFN2 and low-LRFN2 groups in TMA. ** $p < 0.01$, **** $p < 0.0001$. MFI, mean fluorescence intensity; BLCA, bladder cancer; LRFN2, leucine-rich repeat and fibronectin type-III domain-containing protein; PD-1, Programmed cell death-1; DAPI, 4',6-diamidino-2-phenylindole; TCF-1, T cell factor-1.

Meanwhile, we performed gradient analysis for multidimensional distances (0–25 μm , 25–50 μm , 50–100 μm , and 100–150 μm) around tumor cells and found that the expression of LRFN2 in tumor cells (CK^+) and counts of CD8^+ , PD-1^+ , and $\text{TCF-1}^+\text{CK}^-$ cells (excluding tumor molecules expressing TCF-1) increased gradually from proximal to distal, indicating spatial exclusivity between LRFN2^+ tumor cells and effective molecules of CD8^+ T cells (figure 3D,E). Finally, the TMA were divided into two groups according to the median fluorescence intensity of LRFN2 expression. We found that the low-LRFN2 group infiltrated more CD8^+ T cells, PD-1^+ cells, and $\text{CD8}^+\text{TCF-1}^+$ cells compared with the high-LRFN2 expression group (figure 3F–H), suggesting that LRFN2 expression in tumor cells is mutually exclusive with the recruitment, infiltration, and differentiation of CD8^+ T cells, which may be the cause of immunotherapy resistance.

LRFN2 restrains T-cell differentiation and function in mouse BLCA cells

To further verify the results at the animal level, we constructed mouse BLCA MB49-shLRFN2-1, MB49-shLRFN2-2 knock-down cell line and the control cell line MB49-shNC, and performed ProcartaPlex multiplex immunoassay on their cell culture supernatants (figure 4A,B). Similar to that in human BLCA cell lines, the expression of *CCL2*, *CCL3*, *CCL4*, *CCL5*, and *CXCL10* were higher in MB49-shLRFN2-1 and MB49-shLRFN2-2. Interestingly, the expression of two immunosuppressive molecules, interleukin (IL)-4 and IL-10, was downregulated in the knockdown group (figure 4B). qRT-PCR analysis of *CCL2*, *CCL3*, *CCL4*, *CCL5*, *CXCL9*, and *CXCL10* also validated these results at the transcriptome level (figure 4C). An in vitro chemotactic assay also demonstrated that CD8^+ T cells showed a stronger migration ability after LRFN2 knockdown by two different shRNAs in MB49 cells (figure 4D). Similarly, MB49-shLRFN2-1 and MB49-shLRFN2-2 induced more cytotoxicity and tumor-killing ability of T cells than the control group, which were assessed using LDH and co-culture assays (figure 4E,F). Subsequently, we found that two LRFN2 knockdown groups in MB49 promoted CD8^+ T cells and CD4^+ T cells differentiation, that is, from $\text{CD44}^+\text{CD62L}^+$ naive T cells into $\text{CD44}^+\text{CD62L}^+$ central memory T cells, and finally differentiated into $\text{CD44}^+\text{CD62L}^-$ effect memory T cells (figure 4G,H).

LRFN2 deficiency promotes CD8^+ T-cell infiltration and differentiation and enhances anti-PD-1 therapy efficacy

Since LRFN2 deletion showed a considerable effect on the TME, we used LRFN2 knockdown and control mouse cell line MB49 to establish a subcutaneous BLCA-bearing model in C57B/L6 mice (figure 5A). We found the deletion of LRFN2 inhibited tumor growth in mice (figure 5B). When the mice reached the ethical endpoint, we measured the tumor volume and weight and found that the tumors in the LRFN2 deficient group were smaller and lighter (figure 5C,D). The tumor was digested into a single-cell suspension and TILs were analyzed using flow cytometry, the gating strategy can be found in online supplemental

figure S22B. We found that more CD8^+ T cells infiltrated the LRFN2 knockout group than the control group, and the differences were statistically significant (figure 5E). In the LRFN2 deletion group, CD8^+ T cells were more likely to transition from $\text{TCF-1}^+\text{PD-1}^-$ naive T cells to $\text{TCF-1}^+\text{PD-1}^+$ precursor exhausted T cells and $\text{TCF-1}^+\text{PD-1}^+$ terminal exhausted T cells (figure 5F). Simultaneously, the $\text{IFN-}\gamma$ and $\text{TNF-}\alpha$ expressed proportion in CD8^+ TILs increased significantly (figure 5H). In addition, knock-down of LRFN2 led to T-cell differentiation, and showed significantly higher expression of ICI indicators T cell immunoreceptor with Ig and ITIM domain (TIGIT) and T cell immunoglobulin domain and mucin domain-3 (TIM-3) than the control group (figure 5I,J). Similar conclusions can also be obtained from in situ perfusion tumorigenesis experiments on BLCA in mice. As shown in online supplemental figure S20A–C, tumors in the LRFN2 deletion group appeared smaller in the bladder than those in the control group, and their proton flux was lower on average (online supplemental figure S20D,E). Similar to flow cytometry results from in situ tumor formation, more CD8^+ T cells were infiltrated in the LRFN2 deletion group compared with the control group. Moreover, the average fluorescence intensity of TCF-1 was significantly decreased, whereas that of PD-1 was significantly increased, suggesting greater differentiation of CD8^+ TILs (online supplemental figure S20F–H).

Owing to the negative association of LRFN2 with immune checkpoints, we focused our attention on the synergistic effect of LRFN2 deficiency with anti-PD-1 therapy. Mice were treated with PD-1 or isotype control therapy on specific days, as described above (figure 6A). The results showed that although the ICI or LRFN2 knockdown slowed tumor growth and prolonged mice survival time, LRFN2 KD combined with ICI had a stronger antitumor effect, thus providing survival benefits (figure 6B–F). When the target endpoint was reached, the tumors were harvested, and some were sliced into frozen sections for immunohistochemical staining. The results indicated that the PD-1+LRFN knock down (KD) group displayed greater CD8^+ T-cell infiltration than the monotherapy group (figure 6E). Digestion of the remaining tumors and analysis of TILs showed that CD8^+ TILs in the PD-1+LRFN KD group were more likely to lose the naive index CD62L and highly expressed proliferation index Ki-67 compared with the single treatment group (figure 6G,H). To rule out off-target effects, another in vivo tumor-bearing experiment in mice using the second shRNA-knockdown tumor cell line were performed. Additionally, the shLRFN2-2 knock-down group of mice was treated with the ICI α -PD-1. The results, as shown in online supplemental figure S21A,B, indicate that the growth rate of both shRNA knockdown tumor cell lines was significantly lower than that of the shNC group. Furthermore, the shLRFN2-2 group exhibited a stronger tumor control ability after the addition of α -PD-1, which is consistent with the findings presented in figure 6. The size and weight of the tumors are shown in online supplemental figure S21C,D. Through these

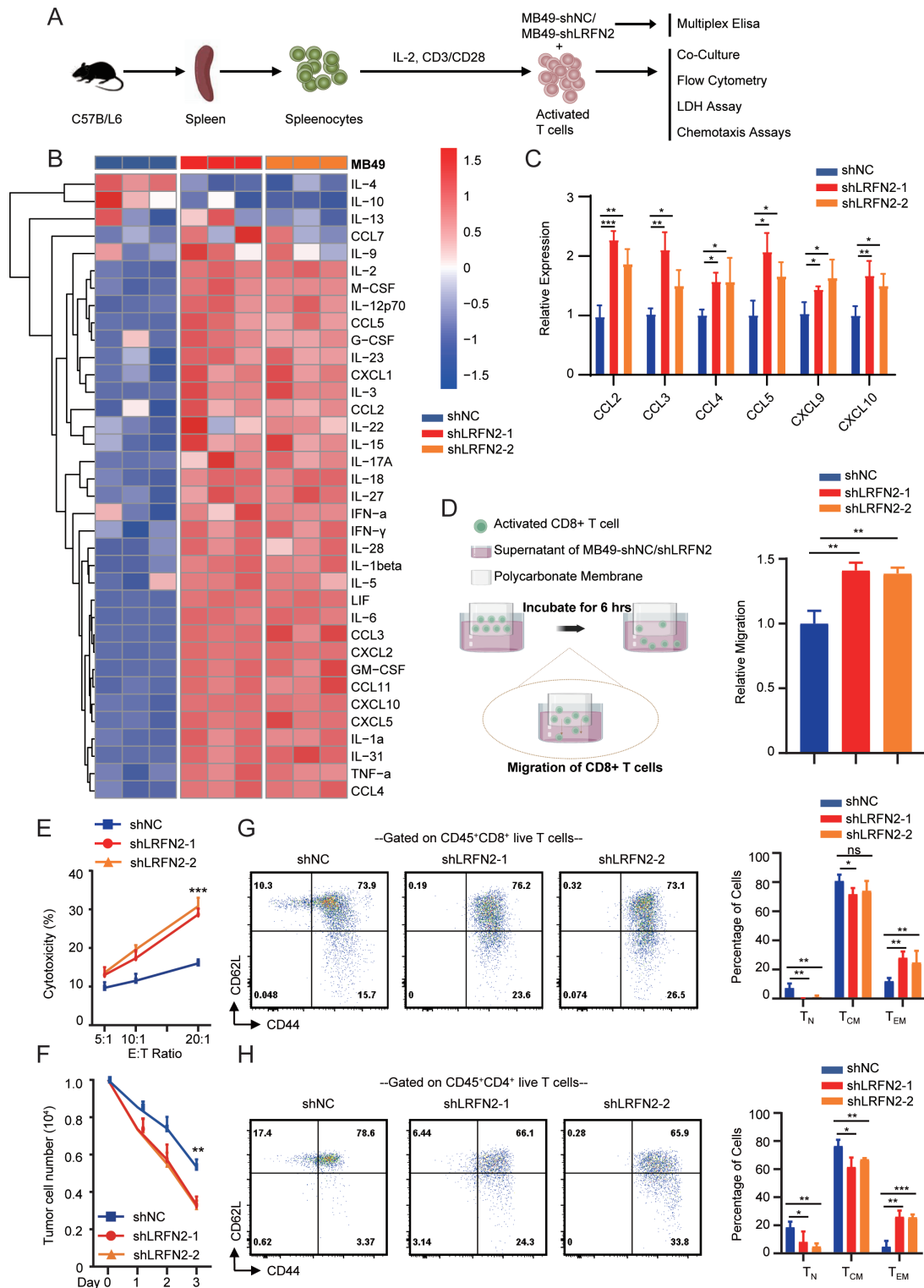


Figure 4 LRFN2 inhibited T-cell differentiation and antitumor ability in mouse bladder cancer in vitro. (A) Flow chart of in vitro studies. (B) Heatmap of the chemokines/cytokines secretion in supernatants of MB49-shNC and MB49-shLRFN2 cells detected by ProcartaPlex multiple immunoassays. (C) Quantitative reverse transcription PCR detected CCL2, CCL3, CCL4, CCL5, CXCL9 and CXCL10 RNA express levels in MB49-shNC and MB49-shLRFN2 cells. (D) Schematic diagram (created with BioRender.com) and histogram of relative migration index of activated CD8⁺ T cells between MB49-shLRFN2 and MB49-shNC. (E–F) The percentage of CD44⁻CD62L⁺ naive T cells (T_N), CD44⁺CD62L⁺ central memory T cells (T_{CM}), and CD44⁺CD62L⁻ effect memory T cells (T_{EM}) in live CD8⁺ T cells (E) and CD4⁺ T cells (F) after co-culture with MB49-shNC and MB49-shLRFN2 cells for 12 hours. (G–H) Line chart showed the T cells cytotoxicity (G) and remained tumor cell numbers (H) after co-culture with MB49-shNC and MB49-shLRFN2 cells for 12 hours. ns, $p > 0.05$, * $p < 0.05$, ** $p < 0.01$, *** $p < 0.001$, **** $p < 0.0001$. IFN, interferon; IL, interleukin; LRFN2, leucine-rich repeat and fibronectin type-III domain-containing protein; TNF, tumor necrosis factor; LDH, lactate dehydrogenase.

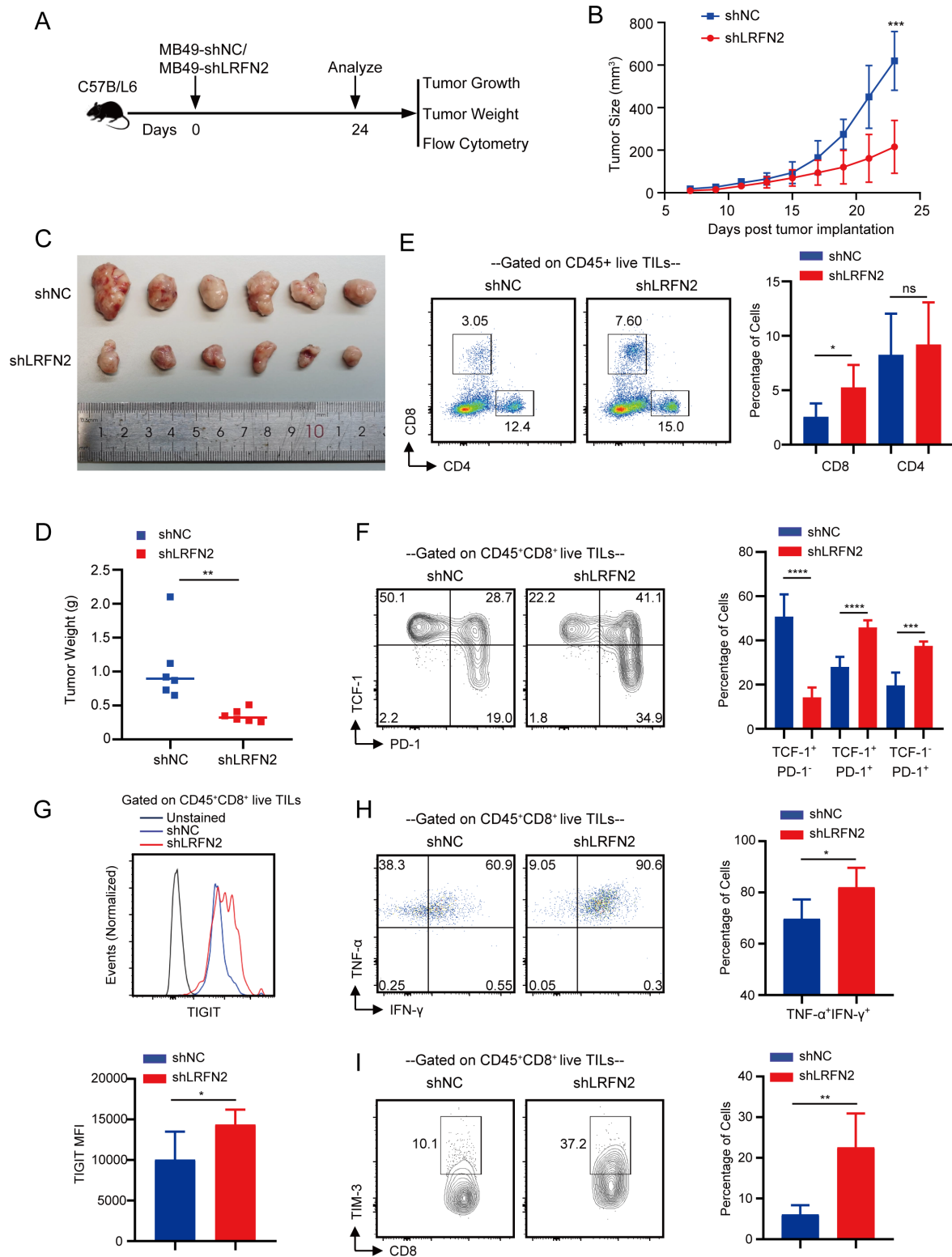


Figure 5 LRFN2 deficiency promote the infiltration and differentiation of CD8⁺ T cells in vivo. (A) Flow chart of in vivo studies. (B) MB49-shLRFN2 and MB49-shNC growth curve in C57BL/6 mice. (C–D) Tumor images (C) and weight (D) of individual groups. (E) The infiltration of CD8⁺ TILs within the live CD45⁺ TILs between MB49-shLRFN2 and MB49-shNC groups. (F) The percentage of TCF-1⁺PD-1⁻ naive T cells, TCF-1⁺PD-1⁺ precursor exhausted T cells, and TCF-1⁻PD-1⁺ terminal exhausted T cells within the live CD45⁺CD8⁺ TILs between MB49-shLRFN2 and MB49-shNC groups. (G) TIGIT expression of live CD8⁺ TILs in different groups. (H) IFN- γ and TNF- α expression of live CD8⁺ TILs in different groups. (I) TIM-3 expression of live CD8⁺ TILs in different groups. ns, p > 0.05, *p < 0.05, **p < 0.01, ***p < 0.001, ****p < 0.0001. IFN, interferon; LRFN2, leucine-rich repeat and fibronectin type-III domain-containing protein; TNF, tumor necrosis factor; PD-1, Programmed cell death-1; TIM-3, T cell immunoglobulin domain and mucin domain-3; MFI, Mean fluorescence intensity; TCF-1, T cell factor-1; TILs, Tumor infiltrating lymphocytes; TIGIT, T cell immunoglobulin and ITIM domain.

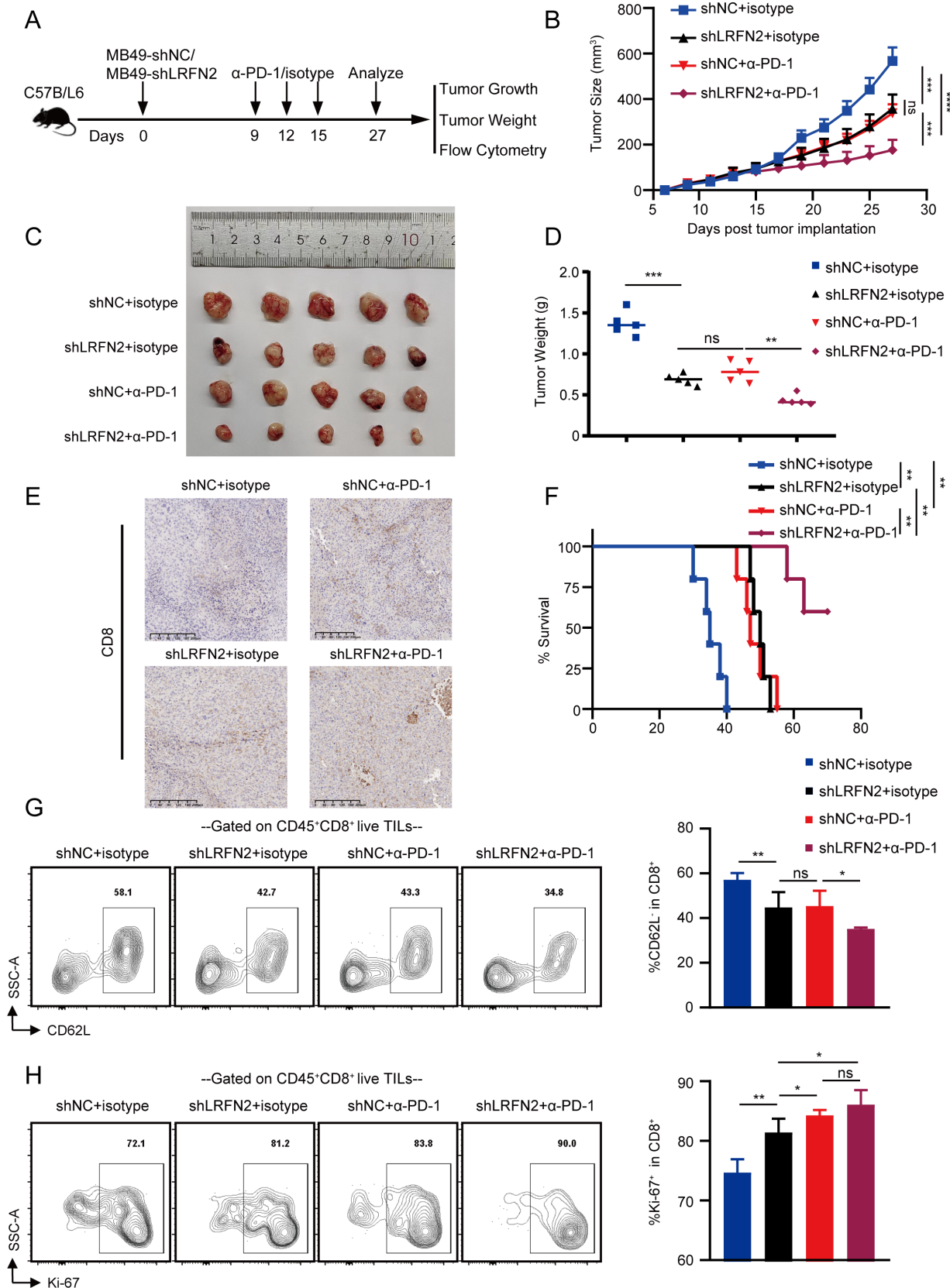


Figure 6 LRFN2 deficiency enhanced the efficacy of anti-PD-1 therapy of bladder cancer in mice. (A) Flow chart of the study. (B) Tumor growth curve among different groups. (C–D) Tumor images (C) and weight (D) of individual groups. (E) Representative IHC images of CD8 staining in individual groups. (F) Mice survival curve of different groups. (G) Percentage of CD62L⁺ cells within the live CD45⁺CD8⁺ TILs between different groups. (H) Ki-67⁺ cells proportion within the live CD45⁺CD8⁺ TILs between different groups. ns, $p > 0.05$, * $p < 0.05$, ** $p < 0.01$, *** $p < 0.001$, **** $p < 0.0001$. LRFN2, leucine-rich repeat and fibronectin type-III domain-containing protein; TILs, Tumor Infiltrating Lymphocytes; IHC, Immunohistochemistry; PD-1, Programmed cell death-1.

experiments, we have demonstrated that shLRFN2-1 and shLRFN2-2 have similar regulatory effects on the immune microenvironment of tumors, thus ruling out the possibility of off-target effects associated with a single shRNA.

Collectively, we found that the deletion of LRFN2 promoted the infiltration and differentiation of TILs, which also enhanced anti-PD-1 therapy efficacy.

Potential of LRFN2 in predicting immunotherapy response in real-world immunotherapy cohorts

The above results indicated that LRFN2 could inhibit the infiltration and functional transition of CD8⁺ T cells, whereas *in vivo* experiments confirmed that LRFN2 deletion combined with anti-PD-1 immunotherapy produced a synergistic therapeutic effect. However, the potential role of LRFN2 in predicting immunotherapy efficacy in the real world remains unclear. Therefore, we constructed a Xiangya BLCA immunotherapy cohort with 51 patients receiving anti-PD-1 therapy, and multiple fluorescence staining was performed on pretreatment samples. Representative staining of LRFN2, CD8, TCF-1, and PD-1 is shown in [figure 7A,B](#) and online supplemental figure S23A,B. High expression of LRFN2 revealed an ICI resistance phenotype, which exhibited a non-inflamed TME and low expression of CD8, TCF-1, and PD-1. Regarding treatment efficacy, complete response (10 cases) and partial response (19 cases) were collated into the response group, and stable disease (16 cases) and progressive disease (6 cases) were collated into the resistance group. In typical CT images before and after anti-PD-1 treatment, we found that the tumor burden was almost completely eliminated in patients with low LRFN2 expression (the response group), whereas there was no definite change in tumor volume in patients with high LRFN2 expression (the resistance group) ([figure 7C](#)). Consistently, immunotherapy response rates were significantly negative correlate with LRFN2 expression ([figure 7D](#)). Moreover, it also showed a negative correlation between LRFN2 expression and disease-free survival (DFS) of patients ([figure 7E](#)). Based on the above experimental results, we selected one patient from the response group and one patient from the resistance group to verify the differential expression of LRFN2 using Immunohistochemistry (IHC) ([figure 7F](#)). We conducted scRNA-sequencing on the tumor samples and analyzed the expression patterns of TILs. As shown in [figure 7G,H](#), TILs can be divided into two groups, exhaust-like and transition-like, according to the differential T-cell gene expression. In terms of the total number of T cells, the response group (low LRFN2 expression) had more exhaust-like TILs, which highly express effector or exhausted markers, such as CCL4, CCL5, JUND, GZMB, CD69, RUNX3, NR4A2, TGFB1, CD44, IL-32, and TIGIT,^{39 41} whereas the resistance group (high LRFN2 expression) had more transition-like TILs, which highly express CD9, S100A11, S100A2, and ELF3 ([figure 7I,J](#)). Analysis of T-cell proportions showed that the LRFN2-high expression group had a higher percentage of transition-like TILs (76.36% vs 9.84%)

and a lower percentage of exhaust-like TILs (23.64% vs 90.16%) compared with the LRFN2-low expression group ([figure 7K](#)). Similarly, patients with low LRFN2 expression showed a stronger positive response rate to immunotherapy in the GSE165252 data set ([figure 7L](#)). Together, these findings showed that LRFN2 can act as a universal predictor and target of immunotherapy response.

DISCUSSION

As a member of the LRFN family, LRFN2 (also known as synaptic adhesive-like molecule 1, SALM1) has previously been notified as a key marker in the nervous system.^{20–22 42 43} LRFN2 can regulate AMPA receptors and associate with SNX27, thus affecting synaptic excitability.²⁰ LRFN2 also had a key role in a range of neurological disorders, such as schizophrenia and Alzheimer's disease.²¹ Meanwhile, LRFN2 has been shown to interact with N-methyl-D-aspartic acid (NMDAR) and cause polycythemia.^{42 43} However, the role of LRFN2 in tumors was unclear, especially regarding the TME and immunotherapy in BLCA. In this work, we comprehensively revealed the expression modes and immune effects of LRFN2 in BLCA and found that LRFN2 may play an immunosuppressive role in BLCA.

Currently, the main immunotherapy methods include adoptive cell therapy and ICI therapy, with ICIs representing the main treatments for BLCA.^{2 3 27 37 44} As a high immunogenic tumor with abundant tumor mutation burden and neoantigen, many studies have confirmed that immunotherapy based on ICIs can significantly enhance the survival rate of patients with BLCA.^{3 6 7 10} In contrast to strong immune response models, such as acute viral infection or autoimmune diseases, T cells infiltrating tumors often exhibit exhaust-like characteristics as they continuously receive antigen stimulation and cannot clear the antigen.^{45–47} ICIs can act on tumor-infiltrating TCF-1⁺PD-1⁺CD8⁺ T cells (also known as precursor exhausted T cells) to promote their proliferation and transition into TCF-1⁺PD-1⁺CD8⁺ T cells (also known as terminally exhausted T cells), with a stronger cytotoxic effect.^{15 48}

Precursor exhausted T cells are similar to stem cells or memory cells, which seem to have a greater life spans and commonly express memory cell markers, such as TCF-1, BCL-6, or FOXO1.^{49–52} Meanwhile, precursor exhausted T cells lack effector molecules expression, such as perforin and GzmB, which regulate inhibitory receptors expression.⁵¹ Interestingly, PD-1 expression is lower in precursor exhausted T cells than in terminally exhausted T cells.^{37 53–55} Precursor exhausted T cells are considered to have certain stem cell and memory cell properties and thus can self-renew, replicate, and massively expand after exposure to ICIs or vaccine treatment, playing a role in enhancing the immune response.^{38 56} Terminally exhausted T cells are thought to highly express immune checkpoints, such as TIM-3, LAG-3, TIGIT, and PD-1, which secrete effector molecules, such as IFN- γ , TNF- α ,

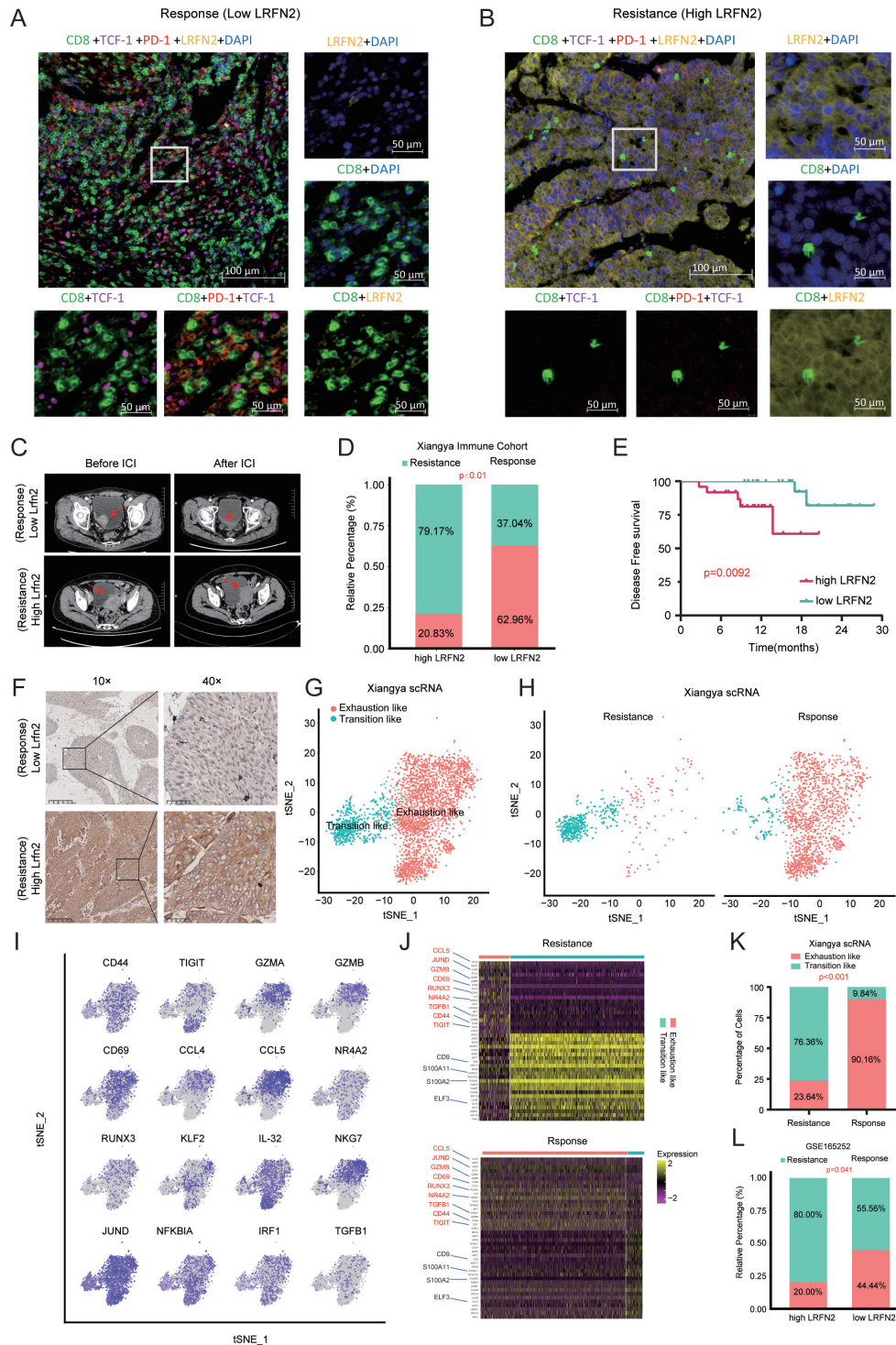


Figure 7 Potential of LRFN2 in predicting immunotherapy response in real-world immunotherapy cohorts. (A–B) Representative image of multicolor staining of staining of LRFN2 (yellow), CD8 (green), TCF-1 (purple), and PD-1 (red) in ICI response (A) and resistance (B) patient with BLCA. (C) Representative CT image for ICI response (upper) and resistance (bottom) patient with BLCA. (D) Relative percentage of resistance and response patients between different LRFN2 expression in the Xiangya immune cohort. (E) Disease-free survival of patients with BLCA between different LRFN2 expression in the Xiangya immune cohort. (F) Immunohistochemical staining images of LRFN2 in the two patients underwent single cell RNA sequencing. (G) tSNE plot of all the single T cells in the Xiangya scRNA-seq. (H) tSNE plot of T cells in resistance group and response group. (I) tSNE plot of differential gene expression on T cells. (J) Heatmap of differential gene expression on T cells between different resistance (upper) and response (bottom) group. (K) Percentage of exhaustion-like and transition-like cells between resistance and response group. (L) Relative percentage of resistance and response patients between different LRFN2 expression in GSE165252. BLCA, bladder cancer; PD-1, Programmed cell death-1; DAPI, 4',6-diamidino-2-phenylindole; tSNE, t-Distributed Stochastic Neighbor Embedding; TCF-1, T cell factor-1; ICI, immune checkpoint inhibitor; LRFN2, leucine-rich repeat and fibronectin type-III domain-containing protein; scRNA-seq, single cell RNA sequencing.

IL-2, perforin, and GzmB, compared with precursor exhausted T cells to achieve stronger antitumor ability but reduce the ability of self-replication and renewal.^{52 57–59} Here, we demonstrated that knockdown of LRFN2 can promote the infiltration, functional transition, and ICI reactivity of CD8⁺ TILs in BLCA, suggesting that LRFN2 deficiency may enhance immunotherapy efficacy by affecting the TME.

Cancer cells, immune cells, fibroblasts, interstitial cells, capillaries, chemokines, and cytokines formed the complex integrated system of TME.^{11 60} Owing to the heterogeneity of the TME, only a minority of patients with BLCA achieved satisfactory efficacy after receiving ICIs in clinical trials, and the majority of patients with BLCA develop primary or secondary resistance to ICIs.² The TME can be divided into inflamed, excluded, and deserted subtypes according to the infiltration of immune cells.²⁷ The non-inflammatory TME is the most important mechanism of immunotherapy resistance because of the scarcity of immunotherapy target molecules and target cells in the non-inflammatory microenvironment.^{16 61–64} The most prominent feature of the non-inflammatory TME is the absence of effector immune cells.^{63 65} The infiltration of these antitumor immune cells depends on the recruitment and chemotaxis of cytokines/chemokines and their receptors.^{65–67} Previous studies showed that high certain molecules (such as BCAT2, β -catenin, and FGFR3) expression in tumor tissues can significantly reduce the expression of chemokines/cytokines.^{68 69} Thus, the ability of tumor tissue to recruit CD8⁺ T cells is reduced, which ultimately induces the formation of a non-inflammatory TME and mediates the immune escape of tumor cells. Hence, we performed a ProcartaPlex multiplex immunoassay and found that most inflammatory cytokines were significantly increased in the LRFN2 knockdown group. Through systematic bioinformatics analysis, we revealed that LRFN2 was associated with the non-inflammatory TME phenotype of BLCA. Furthermore, we comprehensively analyzed several TME-related indicators and found that increased LRFN2 expression formed a non-inflammatory TME, which blocked the cancer immunity cycle, inhibited the cytokine/chemokine spectrum and expression of MHC molecules, and affected the infiltration of tumor-infiltrating immune cells. LRFN2 was negatively correlated with *TIS* and *ICB* effector genes, suggesting that high LRFN2 expression was more likely to be unresponsive to immunotherapy. We further analyzed the immunotherapy response rate in the Xiangya BLCA and public immunotherapy cohorts according to the differential expression of LRFN2. Notably, the results showed significant differences across multiple cohorts, suggesting that LRFN2 could form a non-inflamed TME and may serve as potential biomarkers to predict the immunotherapy efficacy, particularly in BLCA.

Finally, we correlated LRFN2 with BLCA molecular subtypes and key biomarkers for various therapies to guide individual precision therapies. We found that the expression of LRFN2 predicted all classification systems

with high accuracy; we then verified this predicted value using other public databases and our own RNA-seq cohorts. Our findings greatly simplify the molecular classification system and facilitate its clinical application. The basal subtype has been reported to have more cytotoxic lymphocyte and NK cell infiltration, and may be more sensitive to immunotherapy.⁷⁰ The result is consistent with our previous finding that LRFN2 forms a non-inflammatory phenotype with respect to the BLCA molecular subtype. Credible predictions from multiple cohorts showed that patients with BLCA and low LRFN2 expression may benefit more after receiving immunotherapy, chemotherapy, and Erythroblastic Leukemia Viral Oncogene Homolog (ERBB) therapy, whereas patients with high LRFN2 expression are recommended to receive antiangiogenic therapy.

Our study had certain limitations. First, owing to the late clinical application of BLCA immunotherapy, the number of samples included in the Xiangya BLCA and Xiangya immunotherapy cohorts was insufficient. Second, with insufficient follow-up time, we could not directly assess the effect of LRFN2 on overall survival in patients receiving immunotherapy, and only DFS could be used to judge patient efficacy. Third, LRFN2 inhibitors were not used in the functional verification experiments in vivo and in vitro.

Conclusions

In summary, our study revealed LRFN2 as a new target that can be combined with ICIs to provide a potential treatment option for BLCA (online supplemental figure S24).

Author affiliations

¹Department of Urology, Sun Yat-sen University First Affiliated Hospital, Guangzhou, Guangdong, China

²Department of Urology, Xiangya Hospital Central South University, Changsha, Hunan, China

³Department of Breast Surgery, Sun Yat-sen University First Affiliated Hospital, Guangzhou, Guangdong, China

Acknowledgements We would like to thank Dr. Jian Huang for providing MB49 mouse bladder cancer cell lines. We would like to thank TissueGnostics Asia Pacific Limited for their technical support. We would like to thank BioRender.com for creating schematic diagram. We would like to thank Dr Jianming Zeng (University of Macau), and all the members of his bioinformatics team, biotrainee, for generously sharing their experience and codes. We would like to thank OE Biotech Co., Ltd (Shanghai, China) for providing single-cell RNA-seq and Dr Yongbing Ba, Yao Lu, and Hengyun Wang for assistance with bioinformatics analysis.

Contributors AY and JH conceived and designed the study. AY, LF, GH and DD contributed to the study design, performed experiments. AY, JH, MZ, LF, GS, LJ and HL contributed to manuscript writing. XC, TY and JW provided resources. JL, XZ and ZC supervised the work. JL is responsible for the overall content as guarantor. All authors read and approved the final manuscript.

Funding This work was supported by the National Natural Science Foundation of China (81902576, 81873626, 81902592, 82070785, 82103639), Hunan Natural Science Foundation (2020JJ5884) and Hunan Province Young Talents Program (2021RC3027), the Natural Science Foundation of Guangdong Province, China (2023A1515030038), Guangzhou Science and Technology Projects (202201010910).

Competing interests None declared.

Patient consent for publication Not applicable.

Ethics approval The research scheme was approved and monitored by the Ethics Committee of Xiangya Hospital (Item number: 2021101175) and the Ethics Committee of the Clinical Research and Animal Testing Ethics Institute of the First Affiliated Hospital of Sun Yat-sen University (No. 2021001662). Participants gave informed consent to participate in the study before taking part.

Provenance and peer review Not commissioned; externally peer reviewed.

Data availability statement Data are available upon reasonable request.

Supplemental material This content has been supplied by the author(s). It has not been vetted by BMJ Publishing Group Limited (BMJ) and may not have been peer-reviewed. Any opinions or recommendations discussed are solely those of the author(s) and are not endorsed by BMJ. BMJ disclaims all liability and responsibility arising from any reliance placed on the content. Where the content includes any translated material, BMJ does not warrant the accuracy and reliability of the translations (including but not limited to local regulations, clinical guidelines, terminology, drug names and drug dosages), and is not responsible for any error and/or omissions arising from translation and adaptation or otherwise.

Open access This is an open access article distributed in accordance with the Creative Commons Attribution Non Commercial (CC BY-NC 4.0) license, which permits others to distribute, remix, adapt, build upon this work non-commercially, and license their derivative works on different terms, provided the original work is properly cited, appropriate credit is given, any changes made indicated, and the use is non-commercial. See <http://creativecommons.org/licenses/by-nc/4.0/>.

ORCID iDs

Zhenhua Chen <http://orcid.org/0000-0002-8889-5122>

Xiongbing Zu <http://orcid.org/0000-0002-6534-1493>

Junhang Luo <http://orcid.org/0000-0002-5706-0990>

REFERENCES

- Sung H, Ferlay J, Siegel RL, et al. Global cancer Statistics 2020: GLOBOCAN estimates of incidence and mortality worldwide for 36 cancers in 185 countries. *CA Cancer J Clin* 2021;71:209–49.
- Hu J, Chen J, Ou Z, et al. Neoadjuvant Immunotherapy, chemotherapy, and combination therapy in muscle-invasive bladder cancer: a multi-center real-world retrospective study. *Cell Rep Med* 2022;3:100785.
- Cathomas R, Lorch A, Bruins HM, et al. The 2021 updated European Association of Urology guidelines on metastatic urothelial carcinoma. *Eur Urol* 2022;81:95–103.
- Zeng S, Zhang Z, Xu C. Dose-dense methotrexate, vinblastine, doxorubicin, and cisplatin as the gold standard neoadjuvant chemotherapy regimen for patients with nonmetastatic muscle-invasive bladder cancer remains controversial. *J Clin Oncol* 2022;40:3093–4.
- Zhang S. Neoadjuvant programmed cell death protein 1 and chemotherapy in combination in muscle-invasive urothelial cancer: promising, but not deserving to try further. *J Clin Oncol* 2022;40:2656.
- Szabados B, Kockx M, Assaf ZJ, et al. Final results of neoadjuvant atezolizumab in cisplatin-ineligible patients with muscle-invasive urothelial cancer of the bladder. *Eur Urol* 2022;82:212–22.
- Rotte A, Jin JY, Lemaire V. Mechanistic overview of immune checkpoints to support the rational design of their combinations in cancer Immunotherapy. *Ann Oncol* 2018;29:71–83.
- Mariathasan S, Turley SJ, Nickles D, et al. TGF β attenuates tumour response to PD-L1 blockade by contributing to exclusion of T cells. *Nature* 2018;554:544–8.
- Necchi A, Joseph RW, Loriot Y, et al. Atezolizumab in platinum-treated locally advanced or metastatic urothelial carcinoma: post-progression outcomes from the phase II Imvigor210 study. *Annals of Oncology* 2017;28:3044–50.
- Rosenberg JE, Hoffman-Censits J, Powles T, et al. Atezolizumab in patients with locally advanced and metastatic urothelial carcinoma who have progressed following treatment with platinum-based chemotherapy: a single-arm, Multicentre, phase 2 trial. *The Lancet* 2016;387:1909–20.
- Park J, Hsueh P-C, Li Z, et al. Microenvironment-driven metabolic adaptations guiding Cd8⁺ T cell anti-tumor immunity. *Immunity* 2023;56:32–42.
- Wang S, Rong R, Yang DM, et al. Features of tumor-microenvironment images predict targeted therapy survival benefit in patients with EGFR-mutant lung cancer. *J Clin Invest* 2023;133.
- Gajewski TF. The next hurdle in cancer immunotherapy: overcoming the non-T-cell-inflamed tumor microenvironment. *Semin Oncol* 2015;42:663–71.
- Kandalaf LE, Dangaj Laniti D, Coukos G. Immunobiology of high-grade serous ovarian cancer: lessons for clinical translation. *Nat Rev Cancer* 2022;22:640–56.
- Siddiqui I, Schaeuble K, Chennupati V, et al. Intratumoral Tcf1(+)/PD-1(+)/Cd8(+) T cells with stem-like properties promote tumor control in response to vaccination and checkpoint blockade immunotherapy. *Immunity* 2019;50:195–211.
- Yarmarkovich M, Maris JM. When cold is hot: immune checkpoint inhibition therapy for rhabdoid tumors. *Cancer Cell* 2019;36:575–6.
- Park S, Ock CY, Kim H, et al. Artificial intelligence-powered spatial analysis of tumor-infiltrating lymphocytes as complementary biomarker for immune checkpoint inhibition in non-small-cell lung cancer. *J Clin Oncol* 2022;40:1916–28.
- Hornburg M, Desbois M, Lu S, et al. Single-cell dissection of cellular components and interactions shaping the tumor immune phenotypes in ovarian cancer. *Cancer Cell* 2021;39:928–44.
- Zhang B, Wu Q, Li B, et al. Zhou, M(6)A regulator-mediated methylation modification patterns and tumor microenvironment infiltration characterization in gastric cancer. *Mol Cancer* 2020;19:53.
- McMillan KJ, Banks PJ, Hellel FL, et al. Sorting Nexin-27 regulates AMPA receptor trafficking through the synaptic adhesion protein Lrn2. *Elife* 2021;10:e59432.
- Bereczki E, Branca RM, Francis PT, et al. Synaptic markers of cognitive decline in neurodegenerative diseases: a proteomic approach. *Brain* 2018;141:582–95.
- Morimura N, Yasuda H, Yamaguchi K, et al. Autism-like behaviours and enhanced memory formation and synaptic plasticity in Lrn2/ Salm1-deficient mice. *Nat Commun* 2017;8:15800.
- Lie E, Ko JS, Choi SY, et al. Salm4 suppresses excitatory Synapse development by cis-inhibiting Trans-synaptic Salm3-LAR adhesion. *Nat Commun* 2016;7:12328.
- Nam J, Mah W, Kim E. The SALM/Lrn family of Leucine-rich repeat-containing cell adhesion molecules. *Semin Cell Dev Biol* 2011;22:492–8.
- Cai Z, Chen J, Yu Z, et al. Bcat2 shapes a noninflamed tumor microenvironment and induces resistance to anti-PD-1/PD-L1 immunotherapy by negatively regulating proinflammatory chemokines and anticancer immunity. *Adv Sci (Weinh)* 2023;10:2207155.
- Hu J, Othmane B, Yu A, et al. 5Mc regulator-mediated molecular subtypes depict the hallmarks of the tumor microenvironment and guide precision medicine in bladder cancer. *BMC Med* 2021;19:289.
- Hu J, Yu A, Othmane B, et al. Siglec15 shapes a non-inflamed tumor microenvironment and predicts the molecular subtype in bladder cancer. *Theranostics* 2021;11:3089–108.
- Charoentong P, Finotello F, Angelova M, et al. Pan-cancer Immunogenomic analyses reveal genotype-immunophenotype relationships and predictors of response to checkpoint blockade. *Cell Rep* 2017;18:248–62.
- Auslander N, Zhang G, Lee JS, et al. Publisher correction: robust prediction of response to immune checkpoint blockade therapy in metastatic melanoma. *Nat Med* 2018;24:1942.
- Ayers M, Lunceford J, Nebozhyn M, et al. IFN- γ -related mRNA profile predicts clinical response to PD-1 blockade. *J Clin Invest* 2017;127:2930–40.
- Makarevic A, Rapp C, Dettling S, et al. Increased radiation-associated T-cell infiltration in recurrent IDH-mutant glioma. *Int J Mol Sci* 2020;21:7801.
- Saito R, Smith CC, Utsumi T, et al. Molecular subtype-specific immunocompetent models of high-grade urothelial carcinoma reveal differential Neoantigen expression and response to Immunotherapy. *Cancer Res* 2018;78:3954–68.
- Guo CC, Dadhania V, Zhang L, et al. Gene expression profile of the clinically aggressive micropapillary variant of bladder cancer. *Eur Urol* 2016;70:611–20.
- Dadhania V, Zhang M, Zhang L, et al. Meta-analysis of the Luminal and basal subtypes of bladder cancer and the identification of signature immunohistochemical markers for clinical use. *EBioMedicine* 2016;12:105–17.
- Harlin H, Meng Y, Peterson AC, et al. Chemokine expression in melanoma metastases associated with Cd8+ T-cell recruitment. *Cancer Res* 2009;69:3077–85.
- Nagarsheth N, Wicha MS, Zou W. Chemokines in the cancer microenvironment and their relevance in cancer immunotherapy. *Nat Rev Immunol* 2017;17:559–72.
- Fu J, Yu A, Xiao X, et al. Cd4(+) T cell exhaustion leads to adoptive transfer therapy failure which can be prevented by immune checkpoint blockade. *Am J Cancer Res* 2020;10:4234–50.
- McLane LM, Abdel-Hakeem MS, Wherry EJ. Cd8 T cell exhaustion during chronic viral infection and cancer. *Annu Rev Immunol* 2019;37:457–95.

- 39 Chen Z, Ji Z, Ngiow SF, *et al.* TCF-1-centered transcriptional network drives an effector versus exhausted Cd8 T cell-fate decision. *Immunity* 2019;51:840–855.
- 40 Hashimoto M, Kamphorst AO, Im SJ, *et al.* Cd8 T cell exhaustion in chronic infection and cancer: opportunities for interventions. *Annu Rev Med* 2018;69:301–18.
- 41 Crespo J, Sun H, Welling TH, *et al.* T cell Anergy, exhaustion, senescence, and stemness in the tumor microenvironment. *Curr Opin Immunol* 2013;25:214–21.
- 42 Li Y, Kim R, Cho YS, *et al.* Lrnf2-mutant mice display suppressed synaptic plasticity and inhibitory synapse development and abnormal social communication and startle response. *J Neurosci* 2018;38:5872–87.
- 43 Thevenon J, Souchay C, Seabold GK, *et al.* Heterozygous deletion of the Lrnf2 gene is associated with working memory deficits. *Eur J Hum Genet* 2016;24:911–8.
- 44 Babjuk M, Burger M, Capoun O, *et al.* European association of urology guidelines on non-muscle-invasive bladder cancer (TA, T1, and carcinoma in situ). *Eur Urol* 2022;81:75–94.
- 45 Arcia-Anaya D, Elliott T. Stat5A Antagonizes TOX in Cd8(+) T cell exhaustion. *Nat Rev Immunol* 2023;23:73.
- 46 Prokhnjevskaya N, Cardenas MA, Valanparambil RM, *et al.* Cd8⁺ T cell activation in cancer comprises an initial activation phase in lymph nodes followed by Effector differentiation within the tumor. *Immunity* 2023;56:107–24.
- 47 Chow A, Uddin FZ, Liu M, *et al.* The ectonucleotidase Cd39 identifies tumor-reactive Cd8⁺ T cells predictive of immune checkpoint blockade efficacy in human lung cancer. *Immunity* 2023;56:93–106.
- 48 Marabelle A, Tselikas L, de Baere T, *et al.* Intratumoral immunotherapy: using the tumor as the remedy. *Ann Oncol* 2017;28:xii33–43.
- 49 Tsui C, Kretschmer L, Rapelius S, *et al.* MYB orchestrates T cell exhaustion and response to checkpoint inhibition. *Nature* 2022;609:354–60.
- 50 Hashimoto M, Araki K, Cardenas MA, *et al.* PD-1 combination therapy with IL-2 modifies Cd8(+) T cell exhaustion program. *Nature* 2022;610:173–81.
- 51 Kallies A, Zehn D, Utzschneider DT. Precursor exhausted T cells: key to successful immunotherapy. *Nat Rev Immunol* 2020;20:128–36.
- 52 Im SJ, Hashimoto M, Gerner MY, *et al.* Defining Cd8+ T cells that provide the proliferative burst after PD-1 therapy. *Nature* 2016;537:417–21.
- 53 Scott AC, Dündar F, Zumbo P, *et al.* TOX is a critical regulator of tumour-specific T cell differentiation. *Nature* 2019;571:270–4.
- 54 Seo H, Chen J, González-Avalos E, *et al.* TOX and Tox2 transcription factors cooperate with Nr4A transcription factors to impose Cd8(+) T cell exhaustion. *Proc Natl Acad Sci USA* 2019;116:12410–5.
- 55 Alfei F, Kanev K, Hofmann M, *et al.* TOX reinforces the phenotype and longevity of exhausted T cells in chronic viral infection. *Nature* 2019;571:265–9.
- 56 Giles JR, Ngiow SF, Manne S, *et al.* Shared and distinct biological circuits in effector, memory and exhausted Cd8(+) T cells revealed by temporal single-cell transcriptomics and epigenetics. *Nat Immunol* 2022;23:1600–13.
- 57 Blank CU, Haining WN, Held W, *et al.* Defining 'T cell exhaustion. *Nat Rev Immunol* 2019;19:665–74.
- 58 Beltra J-C, Manne S, Abdel-Hakeem MS, *et al.* Developmental relationships of four exhausted Cd8⁺ T cell Subsets reveals underlying transcriptional and epigenetic landscape control mechanisms. *Immunity* 2020;52:825–41.
- 59 Hudson WH, Gensheimer J, Hashimoto M, *et al.* Proliferating transitory T cells with an effector-like transcriptional signature emerge from PD-1⁺ stem-like Cd8⁺ T cells during chronic infection. *Immunity* 2019;51:1043–58.
- 60 Derynck R, Turley SJ, Akhurst RJ. TGFβ biology in cancer progression and immunotherapy. *Nat Rev Clin Oncol* 2021;18:9–34.
- 61 Gupta VK, Pandey S, Lavana S. "Targeting Irak4 signaling in PDAC: turning the "cold" tumors to "hot" ones". *Gastroenterology* 2022;162:1837–9.
- 62 Yuen V-H, Chiu D-C, Law C-T, *et al.* Using mouse liver cancer models based on somatic genome editing to predict immune checkpoint inhibitor responses. *J Hepatol* 2023;78:376–89.
- 63 Zhang J, Huang D, Saw PE, *et al.* Turning cold tumors hot: from molecular mechanisms to clinical applications. *Trends Immunol* 2022;43:523–45.
- 64 Duan X, Chan C, Lin W. Nanoparticle-mediated Immunogenic cell death enables and potentiates cancer Immunotherapy. *Angew Chem Int Ed Engl* 2019;58:670–80.
- 65 Dangaj D, Bruand M, Grimm AJ, *et al.* Cooperation between constitutive and inducible chemokines enables T cell engraftment and immune attack in solid tumors. *Cancer Cell* 2019;35:885–900.
- 66 Li J, Fang Y, Zhang Y, *et al.* Supramolecular self-assembly-facilitated aggregation of tumor-specific transmembrane receptors for signaling activation and converting Immunologically cold to hot tumors. *Adv Mater* 2021;33:e2008518.
- 67 Xiao L, Yeung H, Haber M, *et al.* "Immunometabolism: a 'hot' switch for 'cold' pediatric solid tumors". *Trends Cancer* 2021;7:751–77.
- 68 Sweis RF, Spranger S, Bao R, *et al.* Molecular drivers of the non-T-cell-inflamed tumor microenvironment in urothelial bladder cancer. *Cancer Immunol Res* 2016;4:563–8.
- 69 Korpai M, Puyang X, Jeremy Wu Z, *et al.* Evasion of Immunosurveillance by genomic alterations of PPARγ/RXRα in bladder cancer. *Nat Commun* 2017;8:103.
- 70 Kamoun A, de Reyniès A, Allory Y, *et al.* A consensus molecular classification of muscle-invasive bladder cancer. *Eur Urol* 2020;77:420–33.